ACS APPLIED MATERIALS & INTERFACES

Research Article

www.acsami.org

Durable Pt Electrocatalyst Supported on a 3D Nanoporous Carbon Shows High Performance in a High-Temperature Polymer Electrolyte Fuel Cell

Zehui Yang,[†] Isamu Moriguchi,*[,‡] and Naotoshi Nakashima*[,†,§,⊥]

[†]Department of Applied Chemistry, Graduate School of Engineering, Kyushu University, 744 Motooka, Nishi-ku, Fukuoka 819-0395, Japan

[‡]Division of Chemistry and Materials Science, Graduate School of Engineering, Nagasaki University, 1-14 Bunkyo-Machi, Nagasaki 852-8521, Japan

[§]International Institute for Carbon Neutral Energy Research (WPI-I2CNER), Kyushu University, Fukuoka 819-0395, Japan

[⊥]Core Research for Evolutionary Science and Technology (CREST), Japan Science and Technology Agency (JST), 5 Sanbancho, Chiyoda-ku, Tokyo, 102-0075, Japan

Supporting Information

ABSTRACT: In this paper, we used a 3D nanoporous carbon (NanoPC) with a high specific surface area of 1037 m^2/g as a carbon support for high-temperature polymer electrolyte fuel cell, and fabricated an electrocatalyst (NanoPC/PyPBI/Pt) having platinum nanoparticles of ∼2.2 nm diameter deposited on the NanoPC that was wrapped by poly[2,2′-(2,6-pyridine)-5,5′-bibenzimidazole] (PyPBI). Even after 10 000 start-up/shutdown cycles in the range of 1.0 to 1.5 V vs. RHE, the NanoPC/PyPBI/Pt showed almost no loss in electrochemical surface area (ECSA), which indicated much higher durability than those of a CB/PyPBI/Pt (∼32% loss), in which conventional carbon black (CB) was used in place of the NanoPC, and conventional CB/Pt (∼46% loss). The power density of the NanoPC/PyPBI/Pt was 342 mW/cm^2, which was much higher than those of the CB/PyPBI/Pt (183 mW/cm^2) and CB/Pt (115 mW/cm^2).

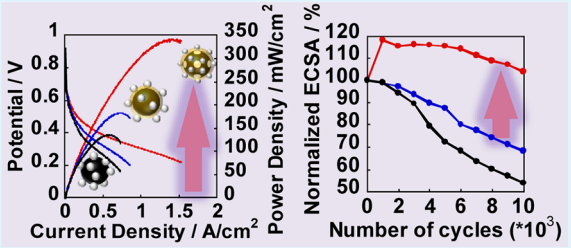

KEYWORDS: *high-temperature PEFC, durability, fuel cell catalyst, nanoporous carbon, polymer wrapping*

INTRODUCTION

Polymer electrolyte fuel cells (PEFCs) have the potential to alleviate major problems associated with the production and consumption of energy, considered as promising, attractive, reliable, and clean energy generation for automotive and stationary applications;[1−4] thus considerable attention has been focused on the high-temperature PEFCs (>100 °C), due to their benefiting PEFCs with higher carbon monoxide (CO) tolerance, faster electrochemical kinetics, and better water management than those of conventional PEFCs.[2,5−9] However, the high-temperature PEFCs also suffer from their low durability in terms of carbon corrosion and platinum nanoparticles (Pt-NPs) aggregation resulting in the detachment of the Pt-NPs from the catalysts and loss in electrochemical surface area (ECSA) as well as the degradation of FC performance.[10−12] Thus, enhancement in durability is highly demanded for the commercialization of the next-generation PEFCs.[13]

Recently, the fabrication and pore arrangement of the nanostructured materials become very important in many fields including PEFCs.[14] Nanoporous carbon (NanoPC) has a porous structure with a higher surface area that has a high potential to be a supporting carbon of PEFCs.[15−17] Meanwhile, the pores provide a pathway to facilitate the mass transport of reactants to the active sites and products of the fuel cell reaction, avoiding the transportation and diffusion limitations, which improves the fuel cell performance.[18−21] Arenz et al. reported that Pt loaded on Ketjenblack showed higher durability than that of Pt loaded on Vulcan, in which the Ketjenblack showed ∼3 times higher specific surface area than that of Vulcan.[22,23] Ogi et al. reported that the Pt-NPs loaded on a porous carbon were more stable than those deposited on CB.[24] Shukla et al. reported that the Pt-NPs deposited on a polymer-wrapped NanoPC were durable against carbon corrosion.[25,26] However, these electrocatalysts are limited in use of the material in high-temperature PFECs due to the lack of proton conduction in the catalyst layer since Nafion ionomers used in such studies work only under 100 °C.[27−29]

We have already reported that poly[2,2′-(2,6-pyridine)-5,5′-bibenzimidazole] (PyPBI) is an efficient dispersant for carbon

Received: February 24, 2015
Accepted: April 22, 2015
Published: April 22, 2015

DOI: 10.1021/acsami.5b01724
ACS Appl. Mater. Interfaces 2015, 7, 9800−9806

supporting materials and provides the anchor sites for the Pt-NPs as well as creating the so-called three-phase boundary (TPB), in which the PyPBI functionalizes as a proton conductor transferring the proton generated from the oxidation of H_2 by the Pt-NPs at high-temperature.[30−33] In this study, we used PyPBI to wrap nanoporous carbon (NanoPC) before Pt-loading as schematically shown in Figure 1 in order to obtain a

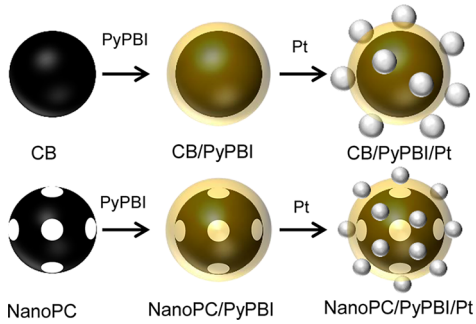

Figure 1. Schematic illumination of preparation of CB/PyPBI/Pt and NanoPC/PyPBI/Pt electrocatalysts.

NanoPC/PyPBI/Pt electrocatalyst. The electrochemical surface area (ECSA), durability, and high temperature fuel cell performance of the prepared electrocatalyst have been measured and compared its performance to the conventional CB/Pt and CB/PyPBI/Pt electrocatalysts.

EXPERIMENTAL SECTION

Materials. LiBr was purchased from Nacalai Tesque Inc. Hydrogen hexachloroplatinate hexahydrate ($H_2PtCl_6{\cdot}6H_2O$), 2-propanol, *N*,*N*-dimethylacetamide (DMAc), ethylene glycol (EG) and 85% phosphoric acid (PA) were purchased from Wako Pure Chemical Industries, Ltd. CB (Vulcan XC-72R) was purchased from Cabot Chemical Co., Ltd. All the chemicals were used as received without any purification. NanoPC was synthesized according to previous reports.[34] PyPBI and poly[2,2′-(2,6-phenyl)-5,5′-bibenzimidazole] (PBI) were synthesized according to previously reported methods.[6]

Synthesis of Electrocatalyst. Ten milligrams of the NanoPC was dispersed in 20 mL of DMAc by sonication for 1 h. Five milligrams of PyPBI was dissolved in 10 mL of DMAc by stirring for 2 h. These solutions were then mixed and sonicated for 2 h, then filtered and dried overnight under vacuum at 80 °C. The deposition of Pt-NPs was carried out by the reduction of $H_2PtCl_6{\cdot}6H_2O$ in EG aqueous solution (EG:H_2O = 3/2,v/v). First, 10 mg of NanoPC/PyPBI (or CB/PyPBI) was dissolved in a 30 mL of EG aqueous solution to which 24 mg of $H_2PtCl_6{\cdot}6H_2O$ was added. The mixture was then refluxed at 140 °C for 6 h under a N_2 atmosphere. By filtration of the dispersion, we obtained the electrocatalysts, which were dried overnight in oven at 80 °C to remove the remained solvent.

Characterization. The X-ray photoelectron spectroscopy (XPS) spectra were measured using an AXIS-ULTRA^{DLD} (Shimadzu) instrument. The TGA measurements were conducted using an EXSTAR 6000, Seiko Inc., at the heating rate of 5 °C/min under 100 mL/min of air flow. The gas adsorption−desorption measurements were conducted after pretreatment at 200 °C for 2 h under high vacuum. The specific surface area and the pore size distribution were determined by the Brunauer−Emmett−Teller (BET) method and Barrett−Joyner−Halenda (BJH) method, respectively, based on the N_2 adsorption isotherm measurements using a BELSORP-mini (BEL Japan, Inc.). The Raman spectra were conducted using RAMANRXN systems (Kaiser optical systems Inc.). The TEM images were measured using a JEM-2010 (JEOL, acceleration voltage of 120 kV) electron microscope. A copper grid with a carbon support (Okenshoji) was used for the TEM observations. X-ray diffraction (XRD) measurements were carried out by using a Rigaku SmartLab diffractometer (Cu, Kα, λ = 1.5406 Å, 40 kV, and 30 mA), the diffraction patterns were collected from 20° to 90° at a scan rate of 1°/min and with a step of 0.01°.

Electrochemical Measurements. The electrochemical measurements were performed using a rotating ring disk electrode attached to an RRDE-3 (Bioanalytical Systems, Inc.) with a conventional three-electrode configuration in a vessel at room temperature. A glassy carbon electrode (GCE) with a geometric surface area of 0.196 cm^2 was used as the working electrode. A Pt wire and an Ag/AgCl were used as the counter and reference electrodes, respectively. The potential of the electrode was controlled by an ALS model DY2323 (BAS) potentiostat. The catalyst suspension was typically prepared as follows. The prepared catalyst (1.0 mg) was ultrasonically dispersed in an 80% aqueous EG solution (2.0 mL) to form a homogeneous suspension. A portion of the dispersion was then cast on a GCE to form a catalyst layer (the loading amount of Pt was controlled at 14 $\mu g/cm^2$). Finally, the cast film on the electrode was air-dried. The cyclic voltammetry (CV) measurements of the electrocatalysts were carried out at the scan rate of 50 mV/s in N_2-saturated 0.1 M $HClO_4$ solution in order to determine the electrochemical surface area (ECSA) values. All the potentials were transformed to the reference hydrogen electrode (RHE). Carbon corrosion durability test was conducted using the protocol[35] of the Fuel Cell Commercialization Conference of Japan (FCCJ) (measured in N_2-saturated 0.1 M $HClO_4$ at room temperature without rotation), in which the potential was hold at 1 V vs. RHE for 30 s and changed to 1.5 V vs. RHE at the scan speed of 0.5 V/s, then the potential was returned to 1 V vs. RHE. After every 1000 cycles, the ECSA values were determined (see the Supporting Information, Figure S1).

Gas Diffusion Electrode (GDE) Fabrication. A GDE was prepared as follows. The electrocatalyst was dispersed in a 50 mL 2-propanol aqueous solution by sonication for 1 h, which was filtered using a carbon gas diffusion layer (GDL) as a filter paper. The Pt loading amount on the GDL was controlled to be 0.45 mg/cm^2. The obtained GDE was dried overnight under vacuum at room temperature to remove the residual solvent.

Preparation of PA-Doped PBI Membrane. In a 50 mL glass bottle, 100 mg of LiBr was dissolved in DMAc (10 mL) to which 200 mg of the PBI polymer was added. The bottle was sealed under N_2, then magnetically stirred at 50 °C for 1 day to reach complete dissolution of the polymer. The DMAc solvent was then evaporated to obtain a solution with a PBI content of ∼4 wt %. The resultant PBI polymer solution was carefully cast on a glass plate using a film applicator (Elcometer 3600, 50 mm strip width). The solvent was then gradually evaporated until the temperature reached 120 °C. The heating process of the formed film was further continued at 120 °C for another 5 h to ensure the removal of the solvent. The PBI film was peeled off from the glass substrate and immersed in hot Milli-Q water for 30 min three times in order to completely remove LiBr. Finally, the PBI membrane was doped in an 85 wt % phosphoric acid solution for 5 days. The membrane thickness of the obtained membrane was determined to be ∼25 μm. The doping level calculated by the weight change of the dry membrane upon doping was 5 H_3PO_4 molecules/repeat unit of the PBI.

Membrane Electrode Assembly (MEA) Fabrication and FC Testing. The MEA was prepared by hot pressing the GDE and the PBI membrane under 2 MPa at 120 °C for 30 s. The active area of the MEA was 1 cm^2. The FC performance of the assembled MEA was evaluated at 120 °C without any external humidification using a computer-controlled fuel cell test system (Model 890e, Scribner Associate, Inc.). The polarization and the power density curves were measured under the atmospheric pressure by flowing dry hydrogen (flow rate; 100 mL/min) and dry air (flow rate; 200 mL/min) at the anode and the cathode, respectively.

RESULTS AND DISCUSSION

Before loading the Pt-NPs on the NanoPC, the morphology was measured by TEM. We observed continuous pores whose diameter was ∼40 nm, which is consistent with the N_2

DOI: 10.1021/acsami.5b01724
ACS Appl. Mater. Interfaces 2015, 7, 9800−9806

adsorption−desorption measurement. The specific surface area of NanoPC was 1037 m^2/g agreed with our previous report (see the Supporting Information, Figures S2a and 3a).[36] The NanoPC also contained large amount of micropores with a diameter of ~2 nm (see Supporting Information, Figure S3c). In this study, the conventional CB/Pt and CB/PyPBI/Pt were used as the baselines. After wrapping by the PyPBI and the Pt-NPs deposition, the XPS spectra of NanoPC/PyPBI/Pt and CB/PyPBI/Pt showed clear N_{1s} peaks at 400 eV derived from PyPBI as shown in Figure 2a. Meanwhile, the peak area of the

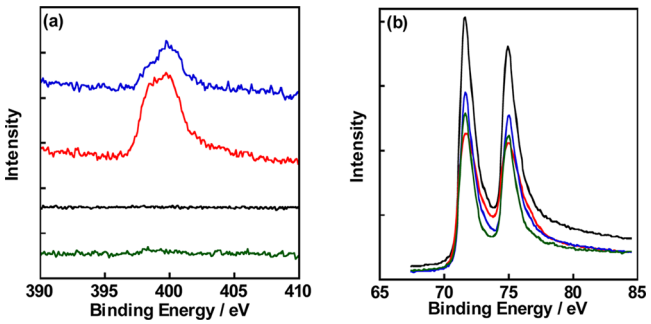

Figure 2. XPS narrow scan of (a) N_{1s} and (b)Pt_{4f} regions of CB/Pt (black line), CB/PyPBI/Pt (blue line), NanoPC/Pt (green line), and NanoPC/PyPBI/Pt (red line).

N_{1s} in the NanoPC/PyPBI/Pt was larger than that in the CB/PyPBI/Pt, which is due to the higher specific surface area of the NanoPC, in which a high amount of the PyPBI was needed to cover all the carbon surfaces. As shown in Figure 2b, two Pt_{4f} peaks at 71.4 and 75.0 eV attributed to the $Pt_{4f7/2}$ and $Pt_{4f5/2}$, respectively, suggesting that the main valence of the Pt species is zero (for survey scans, see the Supporting Information, Figure S4).[37−40] The Pt-NPs were well dispersed on the PyPBI-wrapped NanoPC with the diameter range of 2.2 ± 0.2 nm as shown in Figure 3a, which was smaller than conventional CB/Pt, (3.9 ± 0.6 nm, see the Supporting Information, Figure S5a) and Pt-NPs deposited on the PyPBI-wrapped CB (4.1 ± 0.6 nm, see the Supporting Information, Figure S5b), and the diameters obtained from the TEM were somewhat larger than those calculated from the XRD measurements (1.9, 2.2, and 2.3 nm for NanoPC/PyPBI/Pt, CB/PyPBI/Pt,and CB/Pt, respectively, see the Supporting Information, Figure S6). The obtained smaller Pt-NP-diameters on the PyPBI-wrapped NanoPC would be due to the high surface area of the NanoPC/PyPBI (803 m^2/g) compared to that of the CB/PyPBI (176 m^2/g, see the Supporting Information, Figures S3a and 3b) because all the PyPBI is considered to anchor the Pt-NPs via the Pt−N bonding.[41] The diamter of the Pt-NPs directly deposited on the NanoPC was 2.1 ± 0.2 nm (Figure 3b), which was derived from the high specific surface area of the NanoPC (1037 m^2/g).

The Pt contents in two electrocatalysts determined by the thermal gravimetric analysis (TGA) shown in Figure 4a were

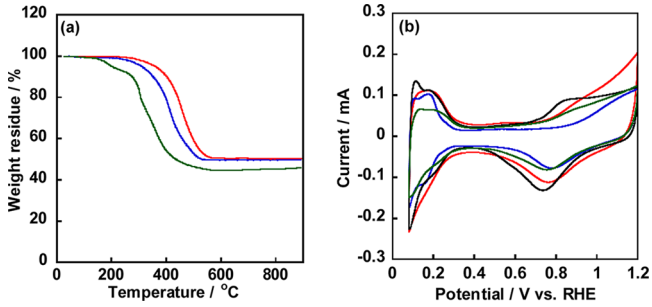

Figure 4. (a) TGA curves of the CB/PyPBI/Pt (blue line), NanoPC/Pt (green line) and NanoPC/PyPBI/Pt (red line). (b) Cyclic voltammetry (CV) curves of CB/Pt (black lline), CB/PyPBI/Pt (blue line), NanoPC/Pt (green line), and NanoPC/PyPBI/Pt (red line) recorded in an N_2-saturated 0.1 M $HClO_4$ solution at the scan rate of 50 mV/s at 25 °C.

50.4 and 49.9 wt % in CB/PyPBI/Pt and NanoPC/PyPBI/Pt, respectively. The decomposition temperature of the CB/PyPBI/Pt was somewhat higher than that of the NanoPC/PyPBI/Pt. This small difference in the decomposition temperature is due to the difference in the carbon supports. We have already reported that the PyPBI started the weight-loss at around 500 °C.[30] The cyclic voltammetry (CV) was recorded in an N_2-saturated 0.1 M $HClO_4$ from 0.1 to 1.2 V vs. RHE as shown in Figure 4b, in which the electrochemical surface areas (ECSAs) were calculated from the hydrogen adsorption peak from 0.1 to 0.35 V vs. RHE, based on eq 1

$$\mathrm{ECSA} = Q_H/210(\mathrm{Pt\ loading\ on\ electrode}) \quad (1)$$

where Q_H is the charge exchanged during the electroadsorption of hydrogen on Pt.[42,43]

The ECSAs were determined to be 60.6, 46.8, and 63.7 m^2/g_{Pt} for CB/Pt, CB/PyPBI/Pt and NanoPC/PyPBI/Pt,

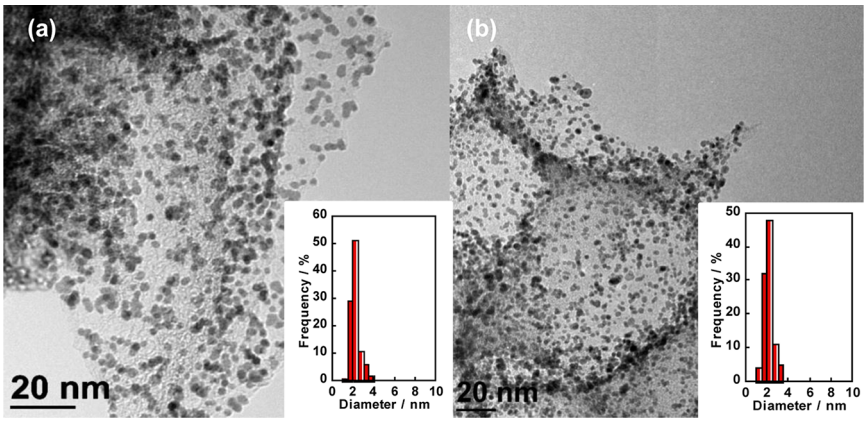

Figure 3. TEM image of (a) as-prepared NanoPC/PyPBI/Pt and (b) NanoPC/Pt. Histograms of particle size distributions (100 particles) are inset.

DOI: 10.1021/acsami.5b01724
ACS Appl. Mater. Interfaces 2015, 7, 9800−9806

respectively. Compared to the CB/PyPBI/Pt, the higher ECSA of NanoPC/PyPBI/Pt was due to the smaller Pt-NPs. The ECSA of the NanoPC/PyPBI/Pt was lower than that of our previous report[44] because the small Pt-NPs were partially deposited onto the micropores of the NanoPC/PyPBI, which were inactive during the ECSA measurement. The NanoPC/PyPBI/Pt showed a comparable ECSA to that of the commercial CB/Pt. While, the ECSA of the NanoPC/Pt was 39 m^2/g_{Pt}, which was much lower than that of the NanoPC/PyPBI/Pt (63.7 m^2/g_{Pt}) because the Pt-NPs size was almost the same as the micropore size and large amounts of the Pt-NPs were deposited onto the micropores of the NanoPC, which decreased the ECSA. Such results indicate that the PyPBI is very important fot improving the efficiency of the Pt-NPs on the NanoPC.

The durability was measured based on the protocol of the Fuel Cell Commercialization Conference of Japan (FCCJ) in which the durability test of the electrocatalyst was simplified to evaluate on the electrode in a N_2-saturated 0.1 M $HClO_4$ electrolyte.[35] Carbon corrosion ($C + 2H_2O \rightarrow CO_2 + 4H^+ + 4e^-$, 0.207 V vs. RHE) was accelerated during the potential cycling from 1 to 1.5 V vs. RHE.[45−47] The hydroquinone−quinone (HQ/Q) redox peaks were observed for all the three electrocatalysts at 0.5 V vs. RHE in Figure 5, implying carbon

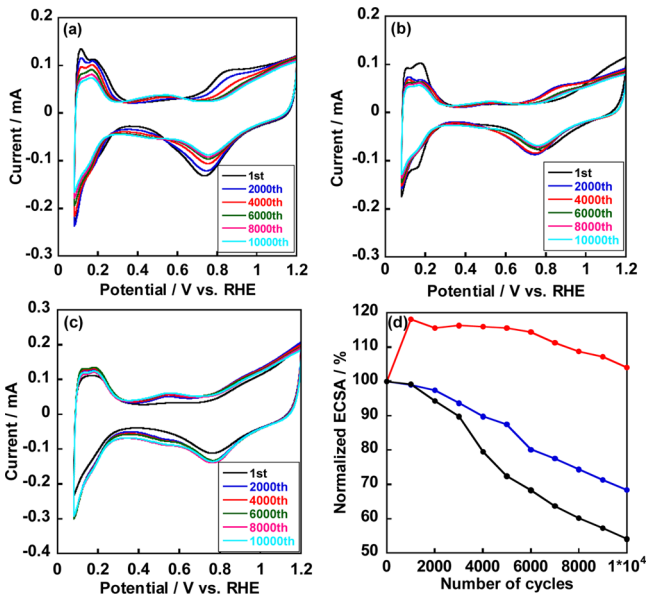

Figure 5. CV curves of the (a) CB/Pt, (b) CB/PyPBI/Pt, and (c) NanoPC/PyPBI/Pt after 2000, 4000, 6000, 8000, and 10 000 potential cycles test. (d) Normalized ECSAs of CB/Pt (black line), CB/PyPBI/Pt (blue line) and NanoPC/PyPBI/Pt (red line) as a function of the number of potential cycles in the range of 1.0−1.5 V vs. RHE.

corrosion.[48] In Figure 5a, b, with the increase in potential cycles, the current of the hydrogen absorption/desorption and Pt oxidation/reduction peaks decreased due to the detachment of the Pt-NPs from the bare CB and CB/PyPBI, leading to 46 and 32% loss in the ECSA, respectively. After wrapping with PyPBI, the polymer protected the CB from serious corrosion. Thus, the CB/PyPBI/Pt showed a higher durability than that of the conventional CB/Pt. In contrast, for the NanoPC/PyPBI/Pt shown in Figure 5c, d, even though the NanoPC shows an identical Raman spectrum as that of the CB, suggesting that the NanoPC has a similar amorphous structure to that of the CB (see the Supporting Information, Figure S7), the ECSA after 10 000 cycles was almost the same as the initial value, indicating that the NanoPc/PyPBI/Pt has the highest durability among the three electrocatalysts.

To clarify the high durability of the NanoPC/PyPBI/Pt, the morphologies of the three electrocatalysts after durability test were observed by TEM. As shown in Figure S5c, d in the Supporting Information, the Pt-NPs in CB/Pt and CB/PyPBI/Pt aggregated to form larger particles with diameters of 5.0 ± 0.5 and 4.9 ± 0.5 nm because of carbon corrosion, which was the predominant factor causing the ECSA loss.[49,50] As shown in Figure 6a, the diameter of the Pt-NPs in the NanoPC/PyPBI/Pt also increased to 3.1 ± 0.3 nm. Surprisingly, as shown in Figure 6b, some smaller Pt-NPs with a diameter of 1.8 ± 0.1 nm were observed (for low-magnification TEM image, see the Supporting Information, Figure S8). The smaller Pt-NPs maintained the identical ECSA for the NanoPC/PyPBI/Pt after the durability test because some Pt-NPs were deposited onto the micropores of the NanoPC, which were unavailable before durability, whereas the micrpores became larger because of the carbon corrosion (see the HQ/Q peaks in Figure 5c), which made the Pt-NPs available for the ECSA measurements as schematically illustrated in Figure 6c. A similar phenomenon was reported by Noto et al., in which the H_2O_2 pretreatment removed the micropores of the support and made the deeply buried electrocatalyst available after the pretreatment.[51,52]

To study the effects of polymer wrapping and porous structure of carbon supporting material on the fuel cell power density, we fabricated the GDEs of three different electrocatalysts according to our previous reports.[12,32,38,40,44] Figure 7 shows the polarization curves of the electrocatalysts operated at 120 °C using dry hydrogen and air under atmospheric pressure for the anode and cathode, respectively, which is a practicable operation condition of the next-generation PEFCs. Before applying the current to the single cell, the open circuit voltages (OCV) were 0.90, 0.92, and 0.91 V for the CB/Pt, CB/PyPBI/Pt and NanoPC/PyPBI/Pt, respectively. The potential of the CB/PyPBI/Pt gradually decreased with the increasing the loaded current compared to that of the CB/Pt. In comparison to the power density of the conventional CB/Pt (115 mW/cm^2), the CB/PyPBI/Pt, it was improved to provide a value of 183 mW/cm^2, which would be due to the homogeneous PyPBI in the catalyst layer functioned as a proton conductor, which enhanced the Pt utilization efficiency. Also the very thin layer of the PyPBI (1−2 nm)[30] has an almost negligible effect in the electron conducitivity of the carbon support. While, by comparison with CB/PyPBI/Pt, the power density of NanoPC/PyPBI/Pt (342 mW/cm^2) was almost 2 times higher than that of the CB/PyPBI/Pt. The enhanced FC performance was due the nanoporous structure of the NanoPC that facilitates the diffusion of the reactant.

CONCLUSIONS

In conclusion, we used a nanoporous carbon (NanoPC) that has a porous structure with a high surface area of 1037 m^2/g to fabricate an electrocatalyst, NanoPC/PyPBI/Pt, having Pt-NPs of ∼2.2 nm diameter that were homogeneously deposited on the PyPBI-wrapped NanoPC. Even after 10 000 start-up/shutdown cycles in the range of 1.0 to 1.5 V vs. RHE, the NanoPC/PyPBI/Pt showed almost no loss in electrochemical surface area (ECSA), indicating very high electrochemical stability. Such behavior was quite different from that of the CB/PyPBI/Pt, and conventional CB/Pt catalysts. The power

DOI: 10.1021/acsami.5b01724
ACS Appl. Mater. Interfaces 2015, 7, 9800−9806

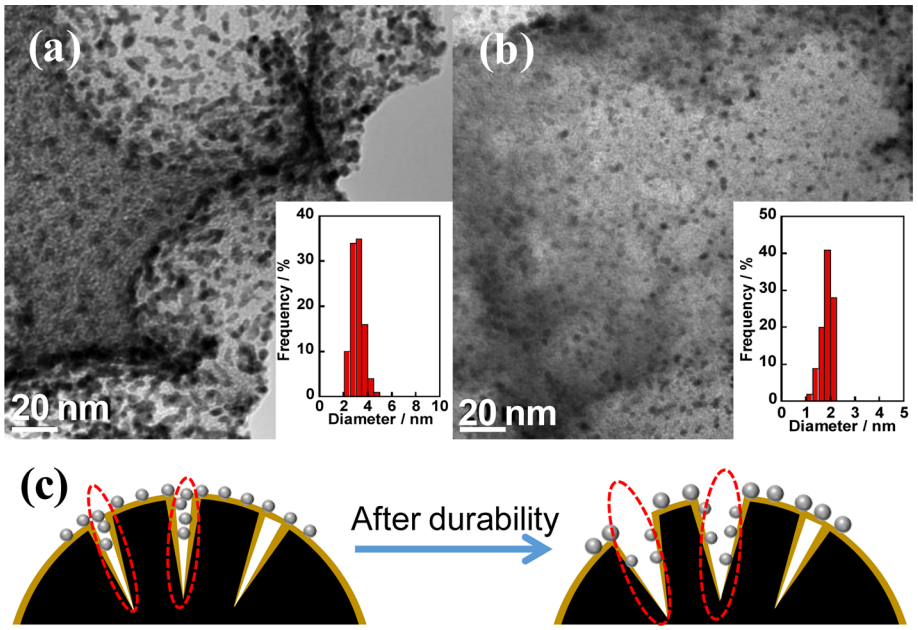

Figure 6. TEM images of the NanoPC/PyPBI/Pt after durability test: (a) larger Pt-NPs area, (b) smaller Pt-NPs area. Inset: histograms of particle size distribution for 100 particles in the TEM images. (c) Schematic illustration of the NanoPC/PyPBI/Pt after the durability test.

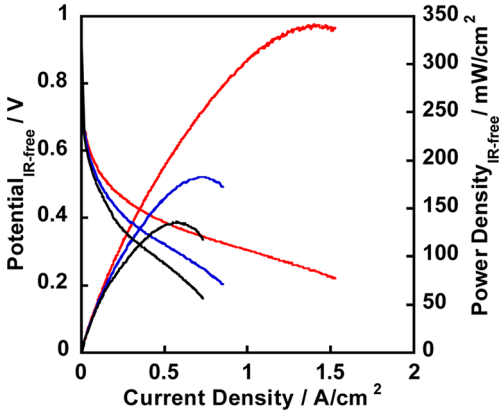

Figure 7. *I*–*V* and power density polarization curves of different MEAs based on CB/Pt (black line), CB/PyPBI/Pt (blue line), and NanoPC/PyPBI/Pt (red line) at 120 °C under a nonhumidified atmosphere.

density of the NanoPC/PyPBI/Pt was 342 mW/cm^2, which was much higher than those of the CB/PyPBI/Pt and CB/Pt because of the unique nanoporous structure that facilitates diffusion of the reactants. The present study provides useful information for the preparation of an electrocatalyst with a high durability and performance in high-temperature PEFCs.

■ ASSOCIATED CONTENT

Supporting Information

XRD spectra, Raman spectra, and TEM images of CB/PyPBI/Pt and CB/PyPBI/Pt before and after durability. The Supporting Information is available free of charge on the ACS Publications website at DOI: 10.1021/acsami.5b01724.

■ AUTHOR INFORMATION

Corresponding Authors

*E-mail: nakashima-tcm@mail.cstm.kyushu-u.ac.jp.
*E-mail: mrgch@nagasaki-u.ac.jp.

Author Contributions

The manuscript was written through contributions of all authors. All authors have given approval to the final version of the manuscript.

Notes

The authors declare no competing financial interest.

■ ACKNOWLEDGMENTS

This work was supported in part by the Low-Carbon Research Network (LCnet) and the Nanotechnology Platform Project (Molecules and Materials Synthesis) of the Ministry of Education, Culture, Sports, Science and Technology (MEXT), Japan, and by The Japan Science and Technology Agency (JST) through its "Center of Innovation Science and Technology based Radical Innovation and Entrepreneurship Program (COI Program). Z.H. Yang acknowledges to China Scholarship Council (CSC) for their support.

■ REFERENCES

(1) Borup, R.; Meyers, J.; Pivovar, B.; Kim, Y. S.; Mukundan, R.; Garland, N.; Myers, D.; Wilson, M.; Garzon, F.; Wood, D.; Zelenay, P.; More, K.; Stroh, K.; Zawodzinski, T.; Boncella, J.; McGrath, J. E.; Inaba, M.; Miyatake, K.; Hori, M.; Ota, K.; Ogumi, Z.; Miyata, S.; Nishikata, A.; Siroma, Z.; Uchimoto, Y.; Yasuda, K.; Kimijima, K.-i.; Iwashita, N. Scientific Aspects of Polymer Electrolyte Fuel Cell Durability and Degradation. *Chem. Rev.* **2007**, *107*, 3904–3951.

(2) Asensio, J. A.; Sanchez, E. M.; Gomez-Romero, P. Proton-conducting Membranes based on Benzimidazole Polymers for High-temperature PEM Fuel cells. A Chemical Quest. *Chem. Soc. Rev.* **2010**, *39*, 3210–39.

(3) Borup, R. L.; Davey, J. R.; Garzon, F. H.; Wood, D. L.; Inbody, M. A. PEM Fuel cell Electrocatalyst Durability Measurements. *J. Power Sources* **2006**, *163*, 76–81.

(4) Rodgers, M. P.; Bonville, L. J.; Kunz, H. R.; Slattery, D. K.; Fenton, J. M. Fuel cell Perfluorinated Sulfonic Acid Membrane Degradation Correlating Accelerated Stress Testing and Lifetime. *Chem. Rev.* **2012**, *112*, 6075–6103.

DOI: 10.1021/acsami.5b01724
ACS Appl. Mater. Interfaces 2015, 7, 9800–9806

(5) Li, Q.; Jensen, J. O.; Savinell, R. F.; Bjerrum, N. J. High temperature Proton Exchange Membranes based on Polybenzimidazoles for Fuel cells. *Prog. Polym. Sci.* **2009**, *34*, 449−477.
(6) Xiao, L.; Zhang, H.; Jana, T.; Scanlon, E.; Chen, R.; Choe, E. W.; Ramanathan, L. S.; Yu, S.; Benicewicz, B. C. Synthesis and Characterization of Pyridine-based Polybenzimidazoles for High temperature Polymer Electrolyte Membrane Fuel cell Applications. *Fuel Cells* **2005**, *5*, 287−295.
(7) Oono, Y.; Fukuda, T.; Sounai, A.; Hori, M. Influence of Operating Temperature on Cell Performance and Endurance of High temperature Proton Exchange Membrane Fuel cells. *J. Power Sources* **2010**, *195*, 1007−1014.
(8) Schmidt, T. J.; Baurmeister, J. Properties of High-temperature PEFC Celtec®-P 1000 MEAs in start/stop Operation Mode. *J. Power Sources* **2008**, *176*, 428−434.
(9) Savadogo, O. Emerging Membranes for Electrochemical Systems: Part II. High temperature Composite Membranes for Polymer Electrolyte Fuel cell (PEFC) Applications. *J. Power Sources* **2004**, *127*, 135−161.
(10) Hara, M.; Lee, M.; Liu, C. H.; Chen, B. H.; Yamashita, Y.; Uchida, M.; Uchida, H.; Watanabe, M. Electrochemical and Raman Spectroscopic Evaluation of Pt/graphitized Carbon Black Catalyst Durability for the start/stop Operating Condition of Polymer Electrolyte Fuel cells. *Electrochim. Acta* **2012**, *70*, 171−181.
(11) Zhao, X.; Hayashi, A.; Noda, Z.; Kimijima, K.; Yagi, I.; Sasaki, K. Evaluation of Change in Nanostructure through the Heat Treatment of Carbon Materials and their Durability for the start/stop Operation of Polymer Electrolyte Fuel cells. *Electrochim. Acta* **2013**, *97*, 33−41.
(12) Berber, M. R.; Hafez, I. H.; Fujigaya, T.; Nakashima, N. Durability Analysis of Polymer-coated Pristine Carbon Nanotube-based Fuel cell Electrocatalysts under Non-humidified Conditions. *J. Mater. Chem. A* **2014**, *2*, 19053−19059.
(13) Weber, A. Z.; Kusoglu, A. Unexplained Transport Resistances for Low-loaded Fuel-cell Catalyst Layers. *J. Mater. Chem. A* **2014**, *2*, 17207−17211.
(14) Ariga, K.; Yamauchi, Y.; Rydzek, G.; Ji, Q.; Yonamine, Y.; Wu, K. C. W.; Hill, J. P. Layer-by-layer Nanoarchitectonics: Invention, Innovation, and Evolution. *Chem. Lett.* **2014**, *43*, 36−68.
(15) Bosco, J. P.; Sasaki, K.; Sadakane, M.; Ueda, W.; Chen, J. G. Synthesis and Characterization of Three-Dimensionally Ordered Macroporous (3DOM) Tungsten Carbide: Application to Direct Methanol Fuel Cells†. *Chem. Mater.* **2010**, *22*, 966−973.
(16) Joo, S. H.; Choi, S. J.; Oh, I.; Kwak, J.; Liu, Z.; Terasaki, O.; Ryoo, R. Ordered Nanoporous Arrays of Carbon Supporting High Dispersions of Platinum Nanoparticles. *Nature* **2001**, *412*, 169−172.
(17) Chang, H.; Joo, S. H.; Pak, C. Synthesis and Characterization of Mesoporous Carbon for Fuel cell Applications. *J. Mater. Chem.* **2007**, *17*, 3078−3088.
(18) Hayashi, A.; Kimijima, K. i.; Miyamoto, J.; Yagi, I. Oxygen Transfer and Storage Processes inside the Mesopores of Platinum-Deposited Mesoporous Carbon Catalyst Thin-Layer Electrode. *J. Phys. Chem. C* **2009**, *113*, 12149−12153.
(19) Minamida, Y.; Zhao, X.; Noda, Z.; Hayashi, A.; Sasaki, K. Characterization of MEAs Fabricated by a Carbon Support with the Nano-Channel Structure. *ECS Trans.* **2013**, *58*, 1105−1111.
(20) Fang, B.; Kim, J. H.; Kim, M. S.; Yu, J. S. Hierarchical Nanostructured Carbons with Meso-macroporosity: Design, Characterization, and Applications. *Acc. Chem. Res.* **2013**, *46*, 1397−1406.
(21) Lai, X.; Halpert, J. E.; Wang, D. Recent Advances in Micro-/nano-structured Hollow Spheres for Energy Applications: From Simple to Complex Systems. *Energy Environ. Sci.* **2012**, *5*, 5604−5618.
(22) Speder, J.; Zana, A.; Spanos, I.; Kirkensgaard, J. J. K.; Mortensen, K.; Arenz, M. On the Influence of the Pt to Carbon Ratio on the Degradation of High Surface Area Carbon Supported PEM Fuel cell Electrocatalysts. *Electrochem. Commun.* **2013**, *34*, 153−156.
(23) Speder, J.; Zana, A.; Spanos, I.; Kirkensgaard, J. J. K.; Mortensen, K.; Hanzlik, M.; Arenz, M. Comparative Degradation Study of Carbon Supported Proton Exchange Membrane Fuel cell Electrocatalysts - The Influence of the Platinum to Carbon Ratio on the Degradation Rate. *J. Power Sources* **2014**, *261*, 14−22.
(24) Balgis, R.; Sago, S.; Anilkumar, G. M.; Ogi, T.; Okuyama, K. Self-Organized Macroporous Carbon Structure Derived from Phenolic Resin via Spray Pyrolysis for High-Performance Electrocatalyst. *ACS Appl. Mater. Interfaces* **2013**, *5*, 11944−11950.
(25) Tintula, K. K.; Jalajakshi, A.; Sahu, A. K.; Pitchumani, S.; Sridhar, P.; Shukla, A. K. Durability of Pt/C and Pt/MC-PEDOT Catalysts under Simulated Start-stop Cycles in Polymer Electrolyte Fuel cells. *Fuel Cells* **2013**, *13*, 158−166.
(26) Tintula, K. K.; Sahu, A. K.; Shahid, A.; Pitchumani, S.; Sridhar, P.; Shukla, A. K. Mesoporous Carbon and Poly(3,4-ethylenedioxythiophene) Composite as Catalyst Support for Polymer Electrolyte Fuel cells. *J. Electrochem. Soc.* **2010**, *157*, B1679−B1685.
(27) Holdcroft, S. Fuel Cell Catalyst Layers: A Polymer Science Perspective. *Chem. Mater.* **2013**, *26*, 381−393.
(28) Aili, D.; Hansen, M. K.; Pan, C.; Li, Q.; Christensen, E.; Jensen, J. O.; Bjerrum, N. J. Phosphoric Acid Doped Membranes based on Nafion ®, PBI and their Blends - Membrane preparation, Characterization and Steam Electrolysis Testing. *Int. J. Hydrogen Energy* **2011**, *36*, 6985−6993.
(29) Mauritz, K. A.; Moore, R. B. State of Understanding of Nafion. *Chem. Rev.* **2004**, *104*, 4535−4585.
(30) Fujigaya, T.; Okamoto, M.; Nakashima, N. Design of an Assembly of Pyridine-containing Polybenzimidazole, Carbon Nanotubes and Pt Nanoparticles for a Fuel cell Electrocatalyst with a High Electrochemically Active Surface Area. *Carbon* **2009**, *47*, 3227−3232.
(31) Okamoto, M.; Fujigaya, T.; Nakashima, N. Design of an Assembly of Poly(benzimidazole), Carbon Nanotubes, and Pt Nanoparticles for a Fuel-cell Electrocatalyst with an Ideal Interfacial Nanostructure. *Small* **2009**, *5*, 735−740.
(32) Matsumoto, K.; Fujigaya, T.; Sasaki, K.; Nakashima, N. Bottom-up Design of Carbon Nanotube-based Electrocatalysts and their Application in High temperature Operating Polymer Electrolyte Fuel cells. *J. Mater. Chem.* **2011**, *21*, 1187−1190.
(33) Yang, Z.; Berber, M. R.; Nakashima, N. A Polymer-coated Carbon Black-based Fuel cell Electrocatalyst with High CO-tolerance and Durability in Direct Methanol Oxidation. *J. Mater. Chem. A* **2014**, *2*, 18875−18880.
(34) Moriguchi, I.; Nakahara, F.; Furukawa, H.; Yamada, H.; Kudo, T. Colloidal Crystal-templated Porous Carbon as a High Performance Electrical Double-layer Capacitor Material. *Electrochem. Solid-State Lett.* **2004**, *7*, A221−A223.
(35) Ohma, A.; Shinohara, K.; Iiyama, A.; Yoshida, T.; Daimaru, A. Membrane and Catalyst Performance Targets for Automotive Fuel Cells by FCCJ Membrane, Catalyst, MEA WG. *ECS Trans.* **2011**, *41*, 775−784.
(36) Yamada, H.; Hirai, T.; Moriguchi, I.; Kudo, T. A Highly Active Pt Catalyst Fabricated on 3D Porous Carbon. *J. Power Sources* **2007**, *164*, 538−543.
(37) Fujigaya, T.; Okamoto, M.; Matsumoto, K.; Kaneko, K.; Nakashima, N. Interfacial Engineering of Platinum Catalysts for Fuel cells: Methanol Oxidation is Dramatically Improved by Polymer Coating on a Platinum Catalyst. *ChemCatChem.* **2013**, *5*, 1701−1704.
(38) Berber, M. R.; Fujigaya, T.; Sasaki, K.; Nakashima, N. Remarkably Durable High Temperature Polymer Electrolyte Fuel Cell Based on Poly(vinylphosphonic acid)-doped Polybenzimidazole. *Sci. Rep.* **2013**, *3*, No. 1764.
(39) Fang, B.; Chaudhari, N. K.; Kim, M. S.; Jung, H. K.; Yu, J. S. Homogeneous Deposition of Platinum Nanoparticles on Carbon Black for Proton Exchange Membrane Fuel cell. *J. Am. Chem. Soc.* **2009**, *131*, 15330−15338.
(40) Berber, M. R.; Fujigaya, T.; Nakashima, N. High-temperature Polymer Electrolyte Fuel cell Using Poly(vinylphosphonic acid) as an Electrolyte shows a Remarkable Durability. *ChemCatChem.* **2014**, *6*, 567−571.
(41) Grove, L. J.; Rennekamp, J. M.; Jude, H.; Connick, W. B. A New Class of Platinum(II) Vapochromic Salts. *J. Am. Chem. Soc.* **2004**, *126*, 1594−1595.

DOI: 10.1021/acsami.5b01724
ACS Appl. Mater. Interfaces 2015, 7, 9800−9806

(42) Fujigaya, T.; Hirata, S.; Nakashima, N. A Highly Durable Fuel cell Electrocatalyst based on Polybenzimidazole-coated Stacked Graphene. *J. Mater. Chem. A* **2014**, *2*, 3888−3893.
(43) Liu, Y.; Mustain, W. E. High Stability, High Activity Pt/ITO Oxygen Reduction Electrocatalysts. *J. Am. Chem. Soc.* **2013**, *135*, 530−533.
(44) Yang, Z.; Hafez, I. H.; Berber, M. R.; Nakashima, N. An Enhanced Anode based on Polymer-Coated Carbon Black for use as a Direct Methanol Fuel Cell Electrocatalyst. *ChemCatChem.* **2015**, *7*, 808−813.
(45) Huang, S.-Y.; Ganesan, P.; Park, S.; Popov, B. N. Development of a Titanium Dioxide-Supported Platinum Catalyst with Ultrahigh Stability for Polymer Electrolyte Membrane Fuel Cell Applications. *J. Am. Chem. Soc.* **2009**, *131*, 13898−13899.
(46) Maass, S.; Finsterwalder, F.; Frank, G.; Hartmann, R.; Merten, C. Carbon Support Oxidation in PEM Fuel cell Cathodes. *J. Power Sources* **2008**, *176*, 444−451.
(47) Huang, S. Y.; Ganesan, P.; Popov, B. N. Titania Supported Platinum Catalyst with High Electrocatalytic Activity and Stability for Polymer Electrolyte Membrane Fuel cell. *Appl. Catal., B* **2011**, *102*, 71−77.
(48) Gharibi, H.; Amani, M.; Pahlavanzadeh, H.; Kazemeini, M. Investigation of Carbon Monoxide Tolerance of Platinum Nanoparticles in the Presence of Optimum Ratio of Doped Polyaniline with para Toluene Sulfonic Acid and their Utilization in a Real Passive Direct Methanol Fuel cell. *Electrochim. Acta* **2013**, *97*, 216−225.
(49) Zana, A.; Speder, J.; Roefzaad, M.; Altmann, L.; Bäumer, M.; Arenz, M. Probing Degradation by IL-TEM: The Influence of Stress Test Conditions on the Degradation Mechanism. *J. Electrochem. Soc.* **2013**, *160*, F608−F615.
(50) Zana, A.; Speder, J.; Reeler, N. E. A.; Vosch, T.; Arenz, M. Investigating the Corrosion of High Surface Area Carbons During start/stop Fuel cell Conditions: A Raman study. *Electrochim. Acta* **2013**, *114*, 455−461.
(51) Di Noto, V.; Negro, E.; Polizzi, S.; Vezzù, K.; Toniolo, L.; Cavinato, G. Synthesis, Studies and Fuel cell Performance of "core−shell" Electrocatalysts for Oxygen Reduction Reaction based on a PtNix Carbon Nitride "shell" and a Pyrolyzed Polyketone Nanoball "core. *Int. J. Hydrogen Energy* **2014**, *39*, 2812−2827.
(52) Negro, E.; Polizzi, S.; Vezzù, K.; Toniolo, L.; Cavinato, G.; Di Noto, V. Interplay between Morphology and Electrochemical Performance of "core−shell" Electrocatalysts for Oxygen Reduction Reaction based on a PtNix Carbon Nitride "shell" and a Pyrolyzed Polyketone Nanoball "core. *Int. J. Hydrogen Energy* **2014**, *39*, 2828−2841.

DOI: 10.1021/acsami.5b01724
ACS Appl. Mater. Interfaces 2015, 7, 9800−9806